Valence- and Conduction-Band Offsets for Atomic-Layer-Deposited Al_2O_3 on (010) $(Al_{0.14}Ga_{0.86})_2O_3$

Chaker Fares, F. Ren, Eric Lambers, David C. Hays, B. P. Gila & S. J. Pearton

Journal of Electronic Materials

ISSN 0361-5235
Volume 48
Number 3

Journal of Elec Materi (2019)
48:1568-1573
DOI 10.1007/s11664-018-06885-x

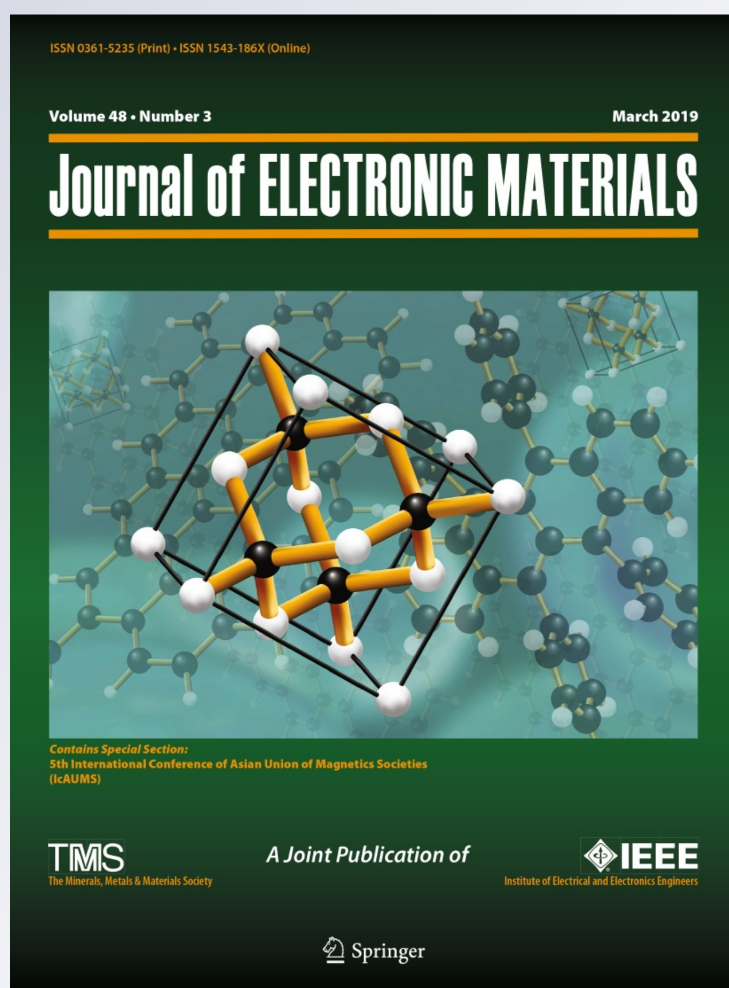

Springer

Your article is protected by copyright and all rights are held exclusively by The Minerals, Metals & Materials Society. This e-offprint is for personal use only and shall not be self-archived in electronic repositories. If you wish to self-archive your article, please use the accepted manuscript version for posting on your own website. You may further deposit the accepted manuscript version in any repository, provided it is only made publicly available 12 months after official publication or later and provided acknowledgement is given to the original source of publication and a link is inserted to the published article on Springer's website. The link must be accompanied by the following text: "The final publication is available at link.springer.com".

Springer

Author's personal copy

Journal of ELECTRONIC MATERIALS, Vol. 48, No. 3, 2019
https://doi.org/10.1007/s11664-018-06885-x
© 2019 The Minerals, Metals & Materials Society

Valence- and Conduction-Band Offsets for Atomic-Layer-Deposited Al_2O_3 on (010) $(Al_{0.14}Ga_{0.86})_2O_3$

CHAKER FARES,[1] F. REN,[1] ERIC LAMBERS,[2] DAVID C. HAYS,[2]
B.P. GILA,[2,3] and S.J. PEARTON[3,4]

1.—Department of Chemical Engineering, University of Florida, Gainesville, FL 32611, USA. 2.—Nanoscale Research Facility, University of Florida, Gainesville, FL 32611, USA. 3.—Department of Materials Science and Engineering, University of Florida, Gainesville, FL 32611, USA. 4.—e-mail: spear@mse.ufl.edu

The wide-bandgap ternary $(Al_xGa_{1-x})_2O_3$ forms a heterostructure system with Ga_2O_3 that is attracting attention for modulation-doped field-effect transistors. The options for gate dielectric on $(Al_xGa_{1-x})_2O_3$ are limited by the need for adequate band offsets at the heterointerface. Al_2O_3 deposited by atomic layer deposition (ALD) is one option due to its large bandgap (6.9 eV). We measured the valence-band offset at the $Al_2O_3/(Al_{0.14}Ga_{0.86})_2O_3$ heterointerface using x-ray photoelectron spectroscopy (XPS). Al_2O_3 was deposited by ALD onto single-crystal β-$(Al_{0.14}Ga_{0.86})_2O_3$ (bandgap 5.0 eV) grown by molecular beam epitaxy (MBE). The valence-band offset was determined to be 0.23 ± 0.04 eV (straddling gap, type I alignment) for ALD Al_2O_3 on β-$(Al_{0.14}Ga_{0.86})_2O_3$. The conduction-band offset was 1.67 ± 0.30 eV, providing good electron confinement.

Key words: Band offset, dielectric, $(AlGa)_2O_3$, atomic layer deposition, band alignment

INTRODUCTION

β-Ga_2O_3 has attracted significant attention recently for applications in power switching electronics and solar-blind ultraviolet (UV) detection.[1–16] Of the phases in which Ga_2O_3 can exist, the β monoclinic polymorph is the most widely studied due to its bandgap of $\sim$ 4.8 eV and availability in large-diameter, bulk wafer form.[1–5] There have been recent reports of excellent device performance for rectifiers, transistors, and solar-blind photodetectors on bulk, epitaxial, and thin flakes of β-Ga_2O_3.[6–21] Ga_2O_3 has a theoretical field breakdown of $\sim$ 8 MV/cm, above the theoretical limits for both SiC and GaN. A three-terminal breakdown voltage of doped lateral Ga_2O_3 metal–oxide–semiconductor field-effect transistor (MOSFETs) of 1850 V was reported for a device with gate–drain distance of 20 μm, while a breakdown voltage of 324 V was obtained for a device with gate–drain separation of 0.8 μm under -32 V gate bias, giving an average lateral gate-to-drain electric field strength of 4.4 ± 0.2 MV/cm.[13] The field plate in these devices comprised a composite of ALD Al_2O_3 and plasma-enhanced chemical vapor-deposited (PECVD) SiO_2 layers.[13] The highest reverse breakdown of a vertical Ga_2O_3 Schottky diode is 2300 V, obtained with dielectric field plates.[14]

The choice of gate dielectric in either MOSFET, metal–insulator–semiconductor field-effect transistor, or field plates for rectifiers is important for optimizing device performance.[17] The band discontinuities form a barrier to carrier transport across the interface, and a $\sim$ 1 eV difference in band edges between the insulating dielectric on the gated area and the channel semiconductor is needed to achieve a sufficient energy barrier to hole and electron leakage current.[2,3,6,17] The majority of published MOSFET, field plate, or passivation work on Ga_2O_3 and related alloys has typically used either ALD Al_2O_3 or HfO_2 or ALD and PECVD SiO_2 and Al_2O_3

(Received September 28, 2018; accepted December 12, 2018; published online January 4, 2019)

Author's personal copy

as the gate dielectrics, with conduction-band differences reported from 1.5 eV to 3.1 eV.[18–37]

Improved MOSFET performance can be achieved by employing β-$(Al_xGa_{1-x})_2O_3$ (for which we use the acronym AGO) monoclinic-phase ternary alloys. This allows the bandgap to be tuned from 4.8 eV to 6 eV, assuming miscibility.[18–23] In perhaps the biggest breakthrough for this material so far, ternary heterostructure field-effect transistors (HFETs) based on an $(Al_xGa_{1-x})_2O_3$ barrier epitaxially grown on a β-Ga_2O_3 buffer on a native substrate exhibited a two-dimensional electron gas, as evidenced by Shubnikov–de Haas oscillations at low temperature.[18–23] In these structures, the value of x is typically 0.12 to 0.17, which produces high-quality epitaxial growth and sharp heterointerfaces and does not create excessive densities of threading dislocations. Figure 1a shows some candidate dielectrics on $(Al_xGa_{1-x})_2O_3$ as a function of bandgap and dielectric constant (K). Note that the variation in dielectric constant over the composition range of AGO is small compared with the scale.[38] Materials with high K are used to reduce the effect of interface traps, and reduce the operating voltage.[4–6,21–24,40–43]

Carey et al.[41] reported the valence-band offsets at Al_2O_3/β-Ga_2O_3 heterointerfaces. The Al_2O_3 was deposited by either ALD or sputtering, and the synthesis method was found to have a strong effect on the resulting band alignment. While the bandgap was 6.9 eV for Al_2O_3 deposited by either method, the valence-band offsets were different for the two deposition methods, with 0.07 ± 0.20 eV (straddling gap, type I alignment) for ALD Al_2O_3 and − 0.86 ± 0.25 eV (staggered gap, type II alignment) for sputtered Al_2O_3. Since the main difference is expected to be the disorder at the dielectric/Ga_2O_3 interface, this shows how the synthesis method can affect the band alignment.

We report herein a determination of the band alignment in the Al_2O_3/β-$(Al_{0.14}Ga_{0.86})_2O_3$ heterostructure, in which amorphous Al_2O_3 was deposited by ALD onto single-crystal $(Al_{0.14}Ga_{0.86})_2O_3$ grown by molecular beam epitaxy (MBE). We employed XPS to determine the valence-band offsets, and by measuring the respective bandgaps of the Al_2O_3 (6.9 eV) and β-$(Al_{0.14}Ga_{0.86})_2O_3$ (5.0 eV), we also determined the conduction-band offset.

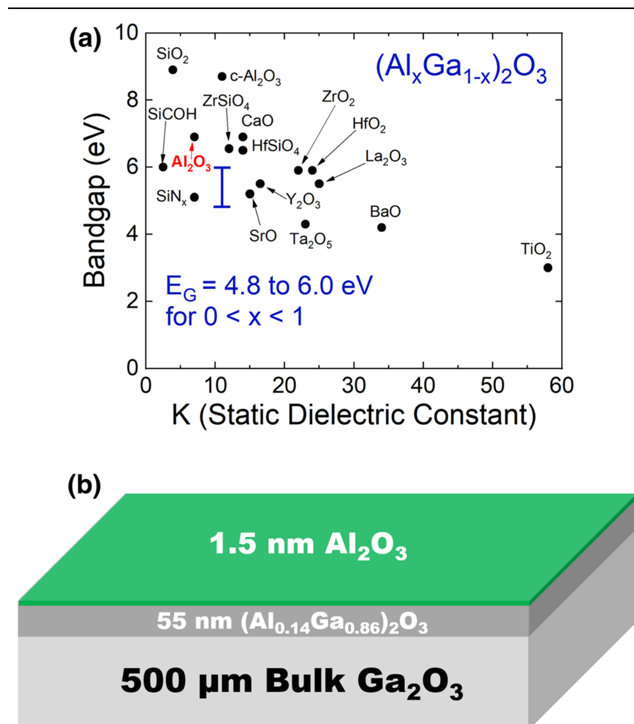

Fig. 1. Dielectric constant and bandgap (a) of candidate dielectrics on the $(Al_xGa_{1-x})_2O_3$ layer structure (b) used in this work.

EXPERIMENTAL PROCEDURES

Al_2O_3 was deposited by ALD on $(Al_{0.14}Ga_{0.86})_2O_3$/$Ga_2O_3$ samples and also quartz substrates. The latter were used for dielectric constant and composition measurements.[39–42] Both thick (200 nm) and thin (1.5 nm) layers of the dielectrics were deposited to measure both the bandgaps and core levels on β-$(Al_{0.14}Ga_{0.86})_2O_3$. For substrate cleaning predeposition, the following rinse sequence was employed: acetone, isopropyl alcohol (IPA), dry N_2, and finally ozone exposure for 15 min. ALD layers were deposited at 200°C in a Cambridge Nano Fiji 200 using a trimethylaluminum source and a remote inductively coupled plasma (ICP) of O_2 at 300 W.

Epi $(Al_{0.14}Ga_{0.86})_2O_3$ was grown by MBE. The composition is representative of heterostructure devices reported to date.[18–23] The AGO was doped with Si to produce an n-type carrier density of 10^{17} cm^{-3} and was 55 nm thick. The donor concentration was determined by electrochemical capacitance–voltage (ECV) profiling at frequency of 740 Hz on calibration samples, and the composition was determined by x-ray diffraction analysis. Since the Si dopant should be ionized at room temperature, the carrier density is closely correlated with the Si donor concentration, a fact confirmed by secondary-ion mass spectrometry. These epitaxial layers were grown on top of Sn-doped (6.3×10^{18} cm^{-3}) bulk β-phase Ga_2O_3 single-crystal substrates (500 μm thick) with (010) surface orientation (Tamura Corporation, Japan) grown by the edge-defined film-fed growth method. The heterostructure sample is shown schematically in Fig. 1.

XPS survey scans determined the chemical state of the Al_2O_3 and β-$(Al_{0.14}Ga_{0.86})_2O_3$ and identified peaks for high-resolution analysis.[44,45] An ULVAC PHI XPS with Al x-ray source (energy 1486.6 eV) with source power of 300 W, analysis size of 20 μm diameter, take-off angle of 50°, and acceptance angle of ± 7° was used. The electron pass energy was 23.5 eV for high-resolution scans and 93.5 eV for survey scans.

Author's personal copy

Charge compensation was performed using an electron flood gun. The adventitious carbon (C-C) line in the C 1*s* spectra at 284.8 eV was used for charge correction. The samples and electron analyzers were electrically grounded to provide a common reference Fermi level. Differential charging[46–53] was not observed with this use of an electron gun.[43]

Reflection electron energy loss spectroscopy (REELS) was used to obtain the Al_2O_3 bandgap,[44–46] using a 1-kV electron beam and hemispherical electron analyzer.

RESULTS AND DISCUSSION

Figure 2 shows the stacked XPS survey scans of thick (200 nm) Al_2O_3, 1.5 nm ALD Al_2O_3 on β-$(Al_{0.14}Ga_{0.86})_2O_3$, and an $(Al_{0.14}Ga_{0.86})_2O_3$ reference sample. The spectra are consistent with past published XPS data on these materials.[26,29–33,39–41] Within the detection limit of XPS, there were no metallic contaminants in the films whose oxides might lower the overall bandgap of the dielectrics and affect the band alignment.

We used linear fitting of the leading edge of the valence band to obtain the valence-band maximum (VBM),[44,45] as shown in Fig. 3a and b for the thick Al_2O_3 and the $(Al_{0.14}Ga_{0.86})_2O_3$, respectively. The VBM was 3.0 ± 0.2 eV for β-$(Al_{0.14}Ga_{0.86})_2O_3$ and 3.25 ± 0.4 eV for the Al_2O_3. The bandgap for the Al_2O_3 was 6.9 ± 0.4 eV according to the REELS data shown in Fig. 4a. The bandgap of the β-$(Al_{0.14}Ga_{0.86})_2O_3$ was determined to be 5.0 ± 0.3 eV from the onset of the plasmon loss feature in the O 1*s* photoemission spectrum shown in Fig. 4b.[44,45] The difference in bandgap between Al_2O_3 and β-Ga_2O_3 is 1.9 eV. The work of Krueger et al.[54] determined the compositional dependence of the bandgap in powder samples of $Al_xGa_{1-x}O$ as a linear dependence on Al content with $E_g = (4.75 + 1.87x)$ eV. This would lead to a value of 5.01 eV, consistent with our result. Their data are based on XPS of polycrystalline samples and represent an averaged standard. Theoretical calculations[27] suggest a dependence of $E_g = (1-x)E_g[Ga_2O_3] + xE_g\ [Al_2O_3] - bx(1-x)$, where b is the bowing parameter. For our sample with $x = 0.14$, this would lead to a bandgap of 5.14 eV, again in rough agreement with our experimental value.

The core-level XPS spectra were used to obtain the valence-band offsets using the standard analysis of measuring the shift of these levels when the dielectric and semiconductor have formed the heterojunction.[44] High-resolution XPS spectra of the VBM–core delta region are shown in Fig. 5a for the β-$(Al_{0.14}Ga_{0.86})_2O_3$ and thick ALD Al_2O_3 (b) samples. Figure 6 shows the XPS spectra for the β-$(Al_{0.14}Ga_{0.86})_2O_3$ to Al_2O_3 core delta regions of the heterostructure samples. These values are summarized in Table I and were used to calculate ΔE_v.

Figure 7 shows the measured nested, type I band alignment of the Al_2O_3/β-$(Al_{0.14}Ga_{0.86})_2O_3$ heterostructure. The valence-band offset is 0.23 ± 0.04 eV, and the conduction-band offset is 1.67 ± 0.30 eV. The valence-band offset is too small for effective hole confinement, but the conduction-band offset would provide good

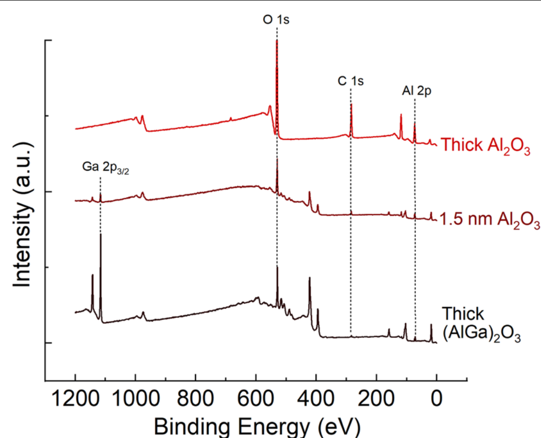

Fig. 2. XPS survey scans of thick ALD Al_2O_3, 1.5 nm ALD Al_2O_3 on $(Al_{0.14}Ga_{0.86})_2O_3$, and an $(Al_{0.14}Ga_{0.86})_2O_3$ reference sample. The intensity is in arbitrary units (a.u.).

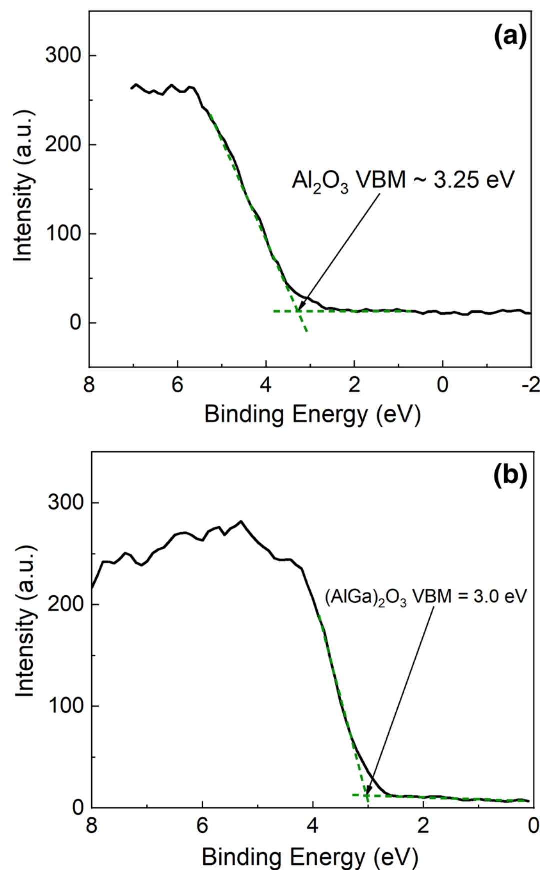

Fig. 3. XPS spectra of core levels to valence-band maximum (VBM) for (a) ALD thick-film Al_2O_3 and (b) reference $(Al_{0.14}Ga_{0.86})_2O_3$. The intensity is in arbitrary units (a.u.).

Author's personal copy

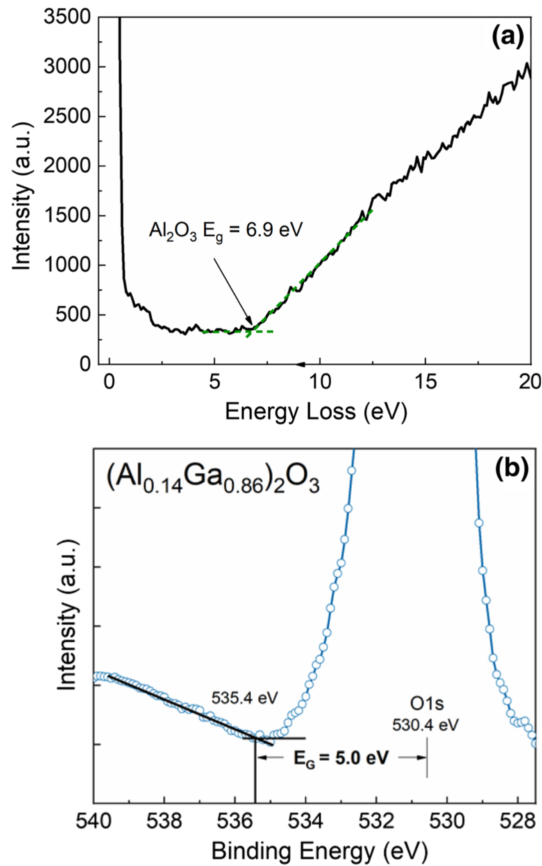

Fig. 4. Bandgap of (a) Al_2O_3 and (b) $(Al_{0.14}Ga_{0.86})_2O_3$ determined by reflection electron energy loss spectra and the onset of the plasmon loss feature in O 1*s* photoemission spectrum, respectively. The intensities are in arbitrary units (a.u.).

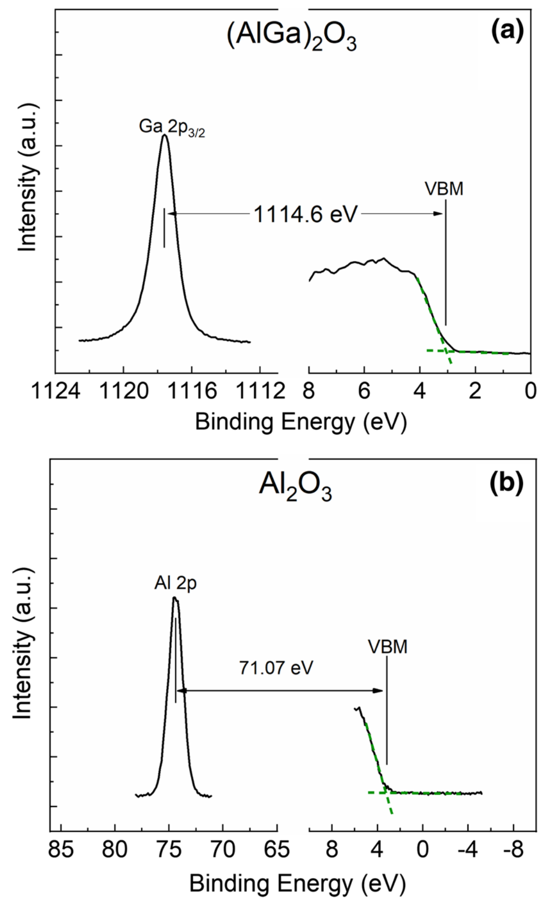

Fig. 5. High-resolution XPS spectra for the vacuum–core delta regions of (a) $(Al_{0.14}Ga_{0.86})_2O_3$ and (b) ALD Al_2O_3. The intensity is in arbitrary units (a.u.).

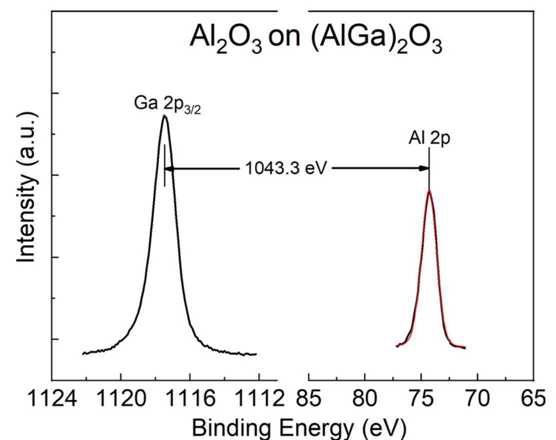

Fig. 6. High-resolution XPS spectra for the $(Al_{0.14}Ga_{0.86})_2O_3$ to Al_2O_3 core delta regions. The intensity is in arbitrary units (a.u.).

electron confinement, even for high-temperature device operation. The low valence-band offset is less of an issue because there are no effective *p*-type dopants in Ga_2O_3. Figure 8 shows a summary of reported band offsets for various dielectrics on $(Al_xGa_{1-x})_2O_3$, including the work of Feng et al.[28] and our group. Additional dielectrics should be examined, especially as higher-Al-content β-$(Al_xGa_{1-x})_2O_3$ is developed for heterostructure transistors, since this will reduce the number of choices that have sufficiently high bandgap to produce type I alignment. Literature on band alignments in all dielectric/semiconductor systems shows that variations of sometimes more than 1 eV depending on interface preparation can be observed.[29–33,39–41,43] These differences are usually seen for the same heterostructure but different deposition methods; i.e., sputtering is more prone to creating interfacial disorder and also results in metallic contamination that affects the bandgap of the dielectric.[43] It will be important to establish the accepted values for band offsets obtained on AGO for controlled deposition methods such as ALD.

CONCLUSIONS

The band alignment at Al_2O_3/β-$(Al_{0.14}Ga_{0.86})_2O_3$ heterojunctions was found to be a nested gap (type I) band offset. This system represents the typical composition of AGO used in heterostructure transistors. The valence-band offset was 0.23 ± 0.04 eV, and the conduction-band offset was 1.67 ± 0.30 eV. The valence-band offset is small and unable to adequately confine holes, whereas the conduction-band offset is sufficient for restricting electron transport.

Author's personal copy

Table I. Summary of measured core levels in these experiments (eV)

Reference $(AlGa)_2O_3$				Reference Al_2O_3				Thin Al_2O_3 on $(AlGa)_2O_3$	
Core Level	VBM	Core Level Peak	Core–VBM	Core Level	VBM	Core Level Peak	Core–VBM	Δ Core Level Ga $2p_{3/2}$—Al $2p$	Valence-Band Offset
Ga $2p_{3/2}$	3.00	1117.60	1114.60	Al $2p$	3.25	74.32	71.07	1043.30	0.23

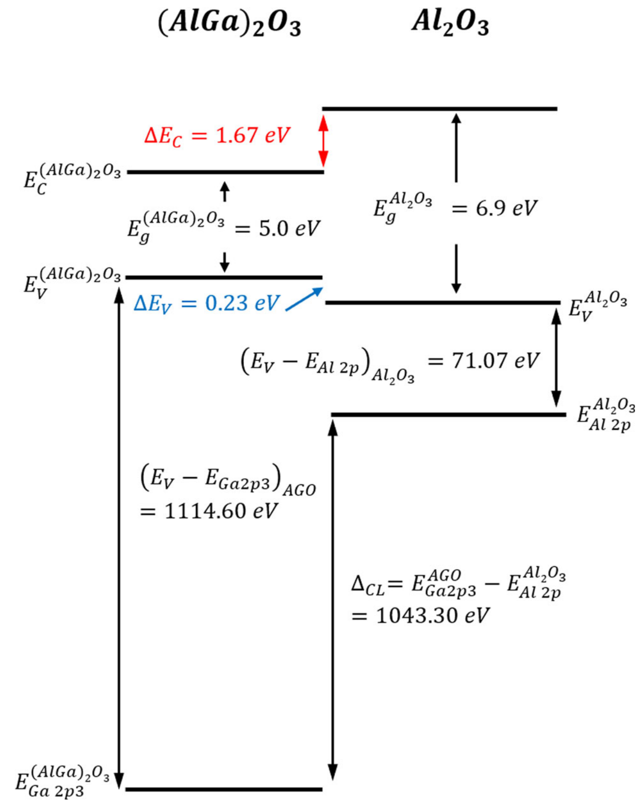

Fig. 7. Band diagrams for the $Al_2O_3/(Al_{0.14}Ga_{0.86})_2O_3$ heterostructure in which the Al_2O_3 was deposited by ALD. The valence-band offset was determined to be 0.23 eV for ALD Al_2O_3 on β-$(Al_{0.14}Ga_{0.86})_2O_3$. The conduction-band offset was 1.67 eV.

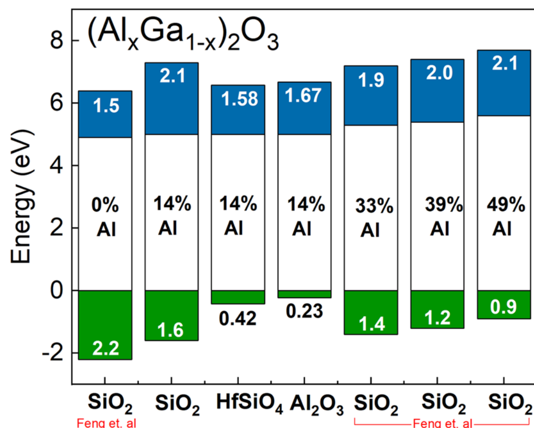

Fig. 8. Reported band offsets for various dielectrics on $(Al_xGa_{1-x})_2O_3$. Data for some of the entries taken from Feng et al.[28]

ACKNOWLEDGMENTS

The project or effort depicted was partially sponsored by the Department of the Defense, Defense Threat Reduction Agency, HDTRA1-17-1-011, monitored by Jacob Calkins.

REFERENCES

1. A. Kuramata, K. Koshi, S. Watanabe, Y. Yamaoka, T. Masui, and S. Yamakoshi, *Jpn. J. Appl. Phys.* 55, 1202A2 (2016).
2. M. Higashiwaki, K. Sasaki, H. Murakami, Y. Kumagai, A. Koukitu, A. Kuramata, T. Masui, and S. Yamakosh, *Semicond. Sci. Technol.* 31, 034001 (2016).
3. J.Y. Tsao, S. Chowdhury, M.A. Hollis, D. Jena, N.M. Johnson, K.A. Jones, R.J. Kaplar, S. Rajan, C.G. Van de Walle, E. Bellotti, C.L. Chua, R. Collazo, M.E. Coltrin, J.A. Cooper, K.R. Evans, S. Graham, T.A. Grotjohn, E.R. Heller, M. Higashiwaki, M.S. Islam, P.W. Juodawlkis, M.A. Khan, A.D. Koehler, J.H. Leach, U.K. Mishra, R.J. Nemanich, R.C.N. Pilawa-Podgurski, J.B. Shealy, Z. Sitar, M.J. Tadjer, A.F. Witulski, M. Wraback, and J.A. Simmons, *Adv. Electron. Mater.* 4, 1600501 (2018).
4. S.J. Pearton, J. Yang, P.H. Cary IV, F. Ren, J. Kim, M.J. Tadjer, and M.A. Mastro, *Appl. Phys. Rev.* 5, 011301 (2018).
5. M. Higashiwaki and G.H. Jessen, *Appl. Phys. Lett.* 112, 060401 (2018).
6. S. Oh, J. Kim, F. Ren, S.J. Pearton, and J. Kim, *J. Mater. Chem. C* 4, 9245 (2016).
7. K.D. Chabak, N. Moser, A.J. Green, D.E. Walker Jr., S.E. Tetlak, E. Heller, A. Crespo, R. Fitch, J.P. McCandless, K. Leedy, M. Baldini, G. Wagner, Z. Galazka, X. Li, and G. Jessen, *Appl. Phys. Lett.* 109, 213501 (2016).
8. A.J. Green, K.D. Chabak, E.R. Heller, R.C. Fitch Jr., M. Baldini, A. Fiedler, K. Irmscher, G. Wagner, Z. Galazka, S.E. Tetlak, A. Crespo, K. Leedy, and G.H. Jessen, *IEEE Electron Device Lett.* 37, 902 (2016).
9. M.J. Tadjer, N.A. Mahadik, V.D. Wheeler, E.R. Glaser, L. Ruppalt, A.D. Koehler, K.D. Hobart, C.R. Eddy Jr., and F.J. Kub, *ECS J. Solid State Sci. Technol.* 5, P468 (2016).
10. K.D. Chabak, J.P. McCandless, N.A. Moser, A.J. Green, K. Mahalingam, A. Crespo, N. Hendricks, B.B. Howe, S.E. Tetlak, K. Leedy, R.C. Fitch, D. Wakimoto, K. Sasaki, A. Kuramata, and G.H. Jessen, *IEEE Electron Device Lett.* 39, 67 (2018).
11. K. Konishi, K. Goto, H. Murakami, Y. Kumagai, A. Kuramata, S. Yamakoshi, and M. Higashiwaki, *Appl. Phys. Lett.* 110, 103506 (2017).
12. M.H. Wong, K. Sasaki, A. Kuramata, S. Yamakoshi, and M. Higashiwaki, *IEEE Electron Device Lett.* 37, 212 (2016).
13. K. Zeng, A. Vaidya, and U. Singisetti, *IEEE Electron Device Lett.* 39, 1385 (2018).
14. J.C. Yang, F. Ren, M.J. Tadjer, and A. Kuramata, *ECS J. Solid State Sci. Technol.* 7, 92 (2018).
15. X. Yan, I.S. Esqueda, J. Ma, J. Tice, H. Wang, X. Yan, I.S. Esqueda, J. Ma, J. Tice, and H. Wang, *Appl. Phys. Lett.* 112, 32101 (2018).
16. Y. Zhang, A. Neal, Z. Xia, C. Joishi, J.M. Johnson, Y. Zheng, S. Bajaj, M. Brenner, D. Dorsey, K. Chabak, G. Jessen, J.

Author's personal copy

Hwang, S. Mou, J.P. Heremans, and S. Rajan, *Appl. Phys. Lett.* 112, 173502 (2018).

17. J. Robertson, *J. Vac. Sci. Technol. B* 18, 1875 (2000).
18. S. Krishnamoorthy, Z. Xia, C. Joishi, Y. Zhang, J. McGlone, J. Johnson, M. Brenner, A.R. Arehart, J. Hwang, and S. Lodha, *Appl. Phys. Lett.* 111, 023502 (2017).
19. E. Ahmadi, O.S. Koksaldi, X. Zheng, T. Mates, Y. Oshima, U.K. Mishra, and J.S. Speck, *Appl. Phys. Express* 10, 071101 (2017).
20. T. Oshima, Y. Kato, N. Kawano, A. Kuramata, S. Yamakoshi, S. Fujita, T. Oishi, and M. Kasu, *Appl. Phys. Express* 10, 035701 (2017).
21. T. Oshima, T. Okuno, N. Arai, Y. Kobayash, and S. Fujita, *Jpn. J. Appl. Phys.* 48, 070202 (2009).
22. Y. Zhang, C. Joishi, Z. Xia, M. Brenner, S. Lodha, and S. Rajan, *Appl. Phys. Lett.* 112, 233503 (2018).
23. F. Zhang, K. Saito, T. Tanaka, M. Nishio, M. Arita, and Q. Guo, *Appl. Phys. Lett.* 105, 162107 (2014).
24. J. Yang, F. Ren, M. Tadjer, S.J. Pearton, and A. Kuramata, 2.3 kV field-plated vertical Ga_2O_3 Schottky rectifiers and 1 A forward current with 650 V reverse breakdown, in: *76th Device Research Conference (DRC)* (2018), pp. 1–2.
25. K. Zeng, A. Vaidya, and U. Singisetti, 710 V breakdown voltage in field plated Ga_2O_3 MOSFET, in: *2018 76th device research conference (DRC)* (2018), pp. 1–2.
26. R. Wakabayashi, M. Hattori, K. Yoshimatsu, K. Horiba, H. Kumigashira, and A. Ohtomo, *Appl. Phys. Lett.* 112, 232103 (2018).
27. H. Peelaers, J.B. Varley, J.S. Speck, and C.G. Van de Walle, *Appl. Phys. Lett.* 112, 242101 (2018).
28. Z. Feng, Q. Feng, J. Zhang, X. Li, L. Fuguo Li, H.-Y.C. Huang, L. Hong-Liang, and Y. Hao, *Appl. Surf. Sci.* 434, 440 (2018).
29. Y. Jia, K. Zheng, J.S. Wallace, J.A. Gardella, and U. Singisetti, *Appl. Phys. Lett.* 106, 102107 (2015).
30. K. Konishi, T. Kamimura, M.H. Wong, K. Sasaki, A. Kuramata, S. Yamakoshi, and M. Higashiwaki, *Phys. Status Solidi B* 253, 623 (2016).
31. T. Kamimura, K. Sasaki, M.H. Wong, D. Krishnamurthy, A. Kuramata, T. Masui, S. Yamakoshi, and M. Higashiwaki, *Appl. Phys. Lett.* 104, 192104 (2014).
32. T.-H. Hung, K. Sasaki, A. Kuramata, D.N. Nath, P.S. Park, C. Polchinski, and S. Rajan, *Appl. Phys. Lett.* 104, 162106 (2014).
33. M. Hattori, T. Oshima, R. Wakabayashi, K. Yoshimatsu, K. Sasaki, T. Masui, A. Kuramata, S. Yamakoshi, K. Horiba, H. Kumigashira, and A. Ohtomo, *Jpn. J. Appl. Phys.* 55, 1202B6 (2016).
34. V.D. Wheeler, D.I. Shahin, M.J. Tadjer, and C.R. Eddy Jr., *ECS J. Solid State Sci. Technol.* 6, Q3052 (2017).
35. W. Wei, Z. Qin, S. Fan, Z. Li, K. Shi, Q. Zhu, and G. Zhang, *Nanoscale Res. Lett.* 7, 562 (2012).
36. S.H. Chang, Z.Z. Chen, W. Huang, X.C. Liu, B.Y. Chen, Z.Z. Li, and E.W. Shi, *Chin. Phys. B* 20, 116101 (2011).
37. Z. Chen, K. Hishihagi, X. Wang, K. Saito, T. Tanaka, M. Nishio, M. Arita, and Q. Guo, *Appl. Phys. Lett.* 109, 102106 (2016).
38. R. Schmidt-Grund, C. Kranert, H. von Wenckstern, V. Zviagin, M. Lorenz, and M. Grundmann, *J. Appl. Phys.* 117, 165307 (2015).
39. P.H. Carey, F. Ren, D.C. Hays, B.P. Gila, S.J. Pearton, S. Jang, and A. Kuramata, *J. Vac. Sci. Technol. B* 35, 041201 (2017).
40. P. Carey, F. Ren, D.C. Hays, B.P. Gila, S.J. Pearton, S. Jang, and A. Kuramata, *Jpn. J. Appl. Phys.* 56, 071101 (2017).
41. P. Carey, F. Ren, D.C. Hays, B.P. Gila, S.J. Pearton, S. Jang, and A. Kuramata, *Vacuum* 142, 52 (2017).
42. D.C. Hays, B.P. Gila, S.J. Pearton, A. Trucco, R. Thorpe, and F. Ren, *J. Vac. Sci. Technol. B* 35, 011206 (2017).
43. D.C. Hays, B.P. Gila, S.J. Pearton, and F. Ren, *Appl. Phys. Rev.* 4, 021301 (2017).
44. E.A. Kraut, R.W. Grant, J.R. Waldrop, and S.P. Kowalczyk, *Phys. Rev. Lett.* 44, 1620 (1980).
45. E. Bersch, M. Di, S. Consiglio, R.D. Clark, G.J. Leusink, and A.C. Diebold, *J. Appl. Phys.* 107, 043702 (2010).
46. H.C. Shin, D. Tahir, S. Seo, Y.R. Denny, S.K. Oh, H.J. Kang, S. Heo, J.G. Chung, J.C. Lee, and S. Tougaard, *Surf. Interface Anal.* 44, 623 (2012).
47. P.H. Carey IV, F. Ren, D.C. Hays, B.P. Gila, S.J. Pearton, S. Jang, and A. Kuramata, *Vacuum* 141, 103 (2017).
48. X. Guo, H. Zheng, S.W. King, V.V. Afanas'ev, M.R. Baklanov, J.-F.D. Marneffe, Y. Nishi, and J.L. Shohet, *Appl. Phys. Lett.* 107, 082903 (2015).
49. H.-K. Dong and L.-B. Shi, *Chin. Phys. Lett.* 33, 016101 (2016).
50. J. Xu, Y. Teng, and F. Teng, *Sci. Rep.* 6, 32457 (2016).
51. M. Yang, R.Q. Wu, Q. Chen, W.S. Deng, Y.P. Feng, J.W. Chai, J.S. Pan, and S.J. Wang, *Appl. Phys. Lett.* 94, 142903 (2009).
52. A. Klein, *J. Phys. C Solid* 27, 134201 (2015).
53. S. Li, F. Chen, R. Schafranek, T.J.M. Bayer, K. Rachut, A. Fuchs, S. Siol, M. Weidner, M. Hohmann, V. Pfeifer, J. Morasch, C. Ghinea, E. Arveux, R. Gunzler, J. Gassmann, C. Korber, Y. Gassenbauer, F. Sauberlich, G.V. Rao, S. Payan, M. Maglione, C. Chirila, L. Pintilie, L. Jia, K. Ellmer, M. Naderer, K. Reichmann, U. Bottger, S. Schmelzer, R.C. Frunza, H. Ursic, B. Malic, W.-B. Wu, P. Erhart, and A. Klein, *Phys. Status Solidi Rapid Res. Lett.* 8, 571 (2014).
54. B.W. Krueger, C.S. Dandeneau, E.M. Nelson, S.T. Dunham, F.S. Ohuchi, and M.A. Olmstead, *J. Am. Ceram. Soc.* 99, 2467 (2016).